Crystal structures of ferredoxin variants exhibiting large changes in [Fe–S] reduction potential

Kaisheng Chen[1–3], Christopher A. Bonagura[1,2], Gareth J. Tilley[2,4], James P. McEvoy[2,4], Yean-Sung Jung[1], Fraser A. Armstrong[4], C. David Stout[5] and Barbara K. Burgess[1]

[1]*Department of Molecular Biology and Biochemistry, University of California, Irvine, California 92697, USA.* [2]*These authors contributed equally to the work.* [3]*Current address: The Genomics Institute of the Novartis Research Foundation, 3115 Merryfield Row, Suite 200, San Diego, California 92121, USA.* [4]*Department of Chemistry, Oxford University, Oxford OX1 3QR, UK.* [5]*Department of Molecular Biology, The Scripps Research Institute, 10550 North Torrey Pines Road, La Jolla, California 92037, USA.*

Published online: 28 January 2002, DOI: 10.1038/nsb751

Elucidating how proteins control the reduction potentials ($E^{0'}$) of [Fe–S] clusters is a longstanding fundamental problem in bioinorganic chemistry. Two site-directed variants of *Azotobacter vinelandii* ferredoxin I (FdI) that show large shifts in [Fe–S] cluster $E^{0'}$ (100–200 mV *versus* standard hydrogen electrode (SHE)) have been characterized. High resolution X-ray structures of F2H and F25H variants in their oxidized forms, and circular dichroism (CD) and electron paramagnetic resonance (EPR) of the reduced forms indicate that the overall structure is not affected by the mutations and reveal that there is no increase in solvent accessibility nor any reorientation of backbone amide dipoles or NH–S bonds. The structures, combined with detailed investigation of the variation of $E^{0'}$ with pH and temperature, show that the largest increases in $E^{0'}$ result from the introduction of positive charge due to protonation of the introduced His residues. The smaller (50–100 mV) increases observed for the neutral form are proposed to occur by directing a $H^{\delta+}$–$N^{\delta-}$ dipole toward the reduced form of the cluster.

Iron–sulfur [Fe–S] proteins are ubiquitous in nature, with ~120 different types identified to date, having functions ranging from essential electron transfer (ET) reactions to regulation of gene expression[1]. This study concerns what is perhaps the most subtle mechanism used by proteins to control the reactivity of specific [Fe–S] clusters: the modification of reduction potential ($E^{0'}$). Thus, even without modifying the cluster type, proteins can modulate the $E^{0'}$ of a specific center by varying its environment[2–10]. For example, $[[4Fe–4S](Cys_4)]^{2-/3-}$ centers ligated *via* a typical CysXXCysXXCys….Cys motif have $E^{0'}$ values between –280 and –715 mV in different proteins[4,11]. The manner in which proteins control reduction potentials of [Fe–S] clusters is a fundamental problem in biological chemistry, with implications for understanding ET energetics and for *de novo* design of [Fe–S] proteins with desired characteristics.

Because the intrinsic reduction potential of a particular type and redox couple of an [Fe–S] cluster is fixed, there is general agreement that the nature of the protein surrounding the cluster must be responsible for variations in reduction potential in different proteins or different locations in the same protein. Both

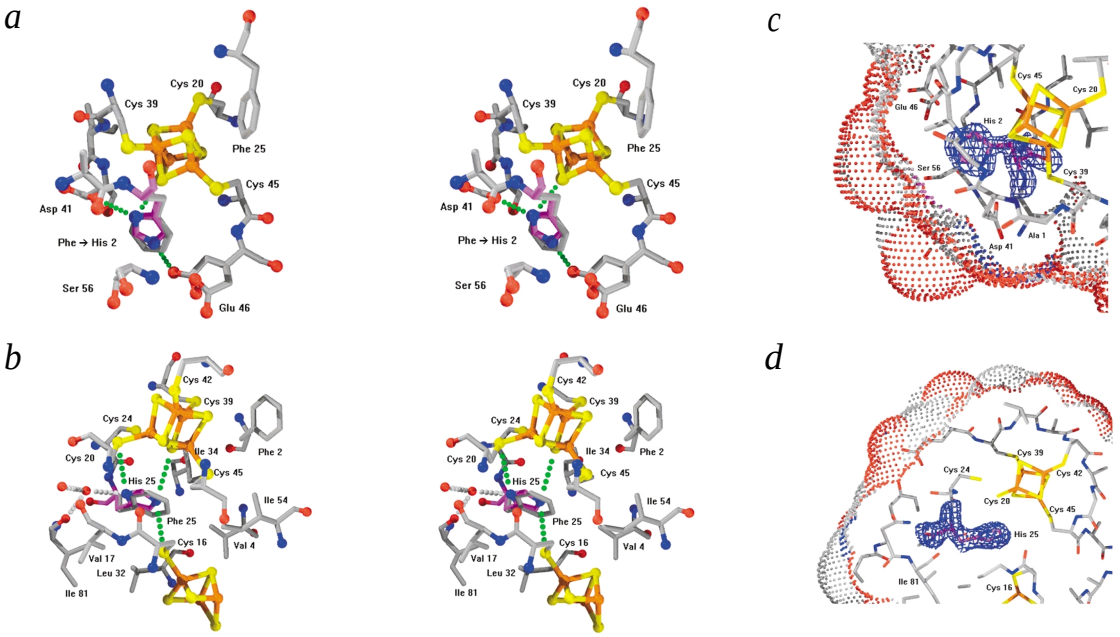

Fig. 1 Crystal structures of FdI mutants showing His 2 and His 25 contacts, solvent accessibility and electron density. Stereo diagrams showing contacts <4 Å from His N atoms to [Fe–S] clusters and hydrogen bonds (green dotted lines). Hydrogen bonds involving water molecules are gray dotted lines. The corresponding Phe residues in native FdI are shown based on least squares superposition of native FdI onto each mutant FdI. Atoms are colored orange (Fe), yellow (S), red (O), blue (N), purple (His C) and gray (C). ***a***, The F2H mutant structure refined at 1.62 Å resolution. Contacts <4 Å from His 2 atoms to sulfur atoms of the $[[4Fe–4S](Cys_4)]^{2-}$ center include Nδ1–S (3.64 Å) and Cγ–S (3.63 Å). Both conformers of Glu 46 are shown. ***b***, The F25H mutant structure refined at 1.75 Å resolution. Contacts <4 Å from His 25 atoms to sulfur atoms of the $[[4Fe–4S](Cys_4)]^{2-}$ center are Nε2–S (3.80 Å) and Cε1–S (3.68 Å), from His 25 atoms to Cys 20 Nδ1–Sγ (3.88 Å) and Cε1–Sγ (3.79 Å), and from His 25 atoms to Cys 16 ($[[3Fe–4S](Cys_3)]^{2-}$ center) Nε2–Sγ (3.74 Å) and Cδ2–Sγ (3.94 Å). The solvent-accessible surface of the ***c***, FdI F2H and ***d***, F25H mutants. The electron density of each His residue is also shown. Atoms and their corresponding surfaces are colored as in (*a*,*b*). His 2 is completely buried except for a small portion of Cε1 (purple dots in (*c*)). His 25 is also completely buried except for a contact of Nδ1 to a water molecule as shown in (*b*). Electron density maps are calculated with σ_A coefficients and contoured at 1.5 σ.

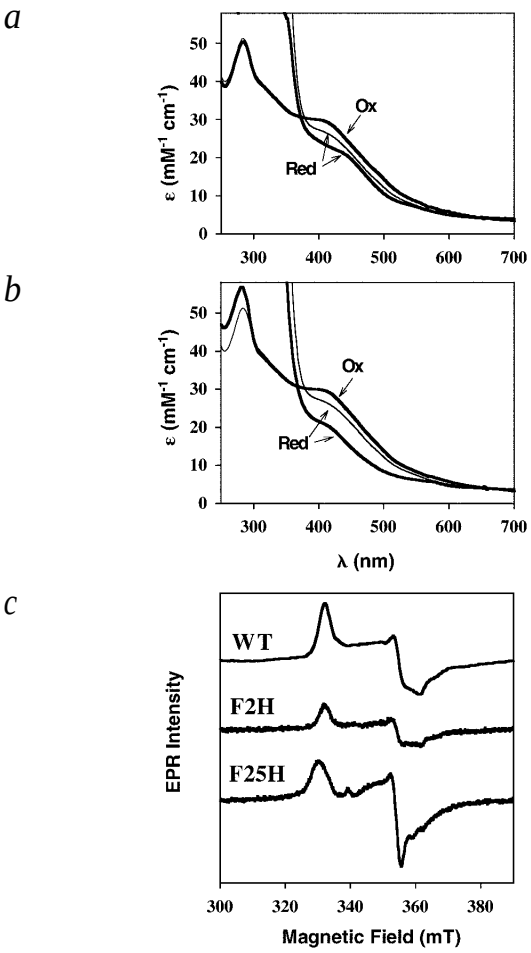

Fig. 2 UV/Vis and EPR spectra of FdI variants. ***a***, UV/Vis spectra of F2H (thick line). For comparison, the spectra of native FdI are also included (thin lines). 'Ox' and 'Red' represent the oxidized and dithionite reduced spectra of the native and F2H FdI, respectively. ***b***, UV/Vis spectra of F25H (thick line). For comparison, the spectra of native FdI are also included (thin lines). 'Ox' and 'Red' represent the oxidized and reduced spectra of the native and F25H, respectively. ***c***, EPR spectra of the [4Fe–4S] clusters of reduced native, F2H, and F25H FdI. The $[[4Fe–4S](Cys_4)]^{2-}$ centers of F2H and F25H FdI were reduced by 2 mM sodium dithionite in 50 mM Tris-HCl, pH 7.4. Under these conditions, the $[[4Fe–4S](Cys_4)]^{2-}$ center of native FdI cannot be reduced; reduction of the native protein was accomplished using the lower potential reductant, 5′-deazariboflavin, EDTA and illumination with visible light. The g values are 2.078, 1.942 and 1.908 for native and F2H, and 2.086, 1.945 and 1.919 for F25H, which also has slightly altered relaxation properties (optimum temperature <8 K) when compared to the native FdI $[[4Fe–4S](Cys_4)]^{3-}$ center, which has an optimum temperature of 12 K.

experimental and theoretical research have been directed toward understanding how proteins control the reduction potentials of [Fe–S] clusters in order to identify what factor(s) is (are) of primary importance[2,4,11–19]. The following have been suggested as candidates: (i) solvent exposure of the cluster; (ii) specific hydrogen bonding, especially involving NH–S bonds; (iii) the proximity and orientation of protein backbone and side chain dipoles; and/or (iv) the proximity and position of charged residues. The purpose of this study is to evaluate the extent to which His residues that are not ligands can influence [Fe–S] cluster $E^{0'}$.

Selection of FdI variants

Our studies focus upon an extremely well-characterized model protein, *Azotobacter vinelandii* ferredoxin I (FdI), which contains one $[[4Fe–4S](Cys_4)]^{2-/3-}$center, with $E^{0'}$ ~–619 mV at pH 7, and one $[[3Fe–4S](Cys_3)]^{2-/3-}$ center (Figure 1). Previous attempts to raise $E^{0'}$ for the $[[4Fe–4S](Cys_4)]^{2-/3-}$ center by modifying surface charged residues were unsuccessful[12], and only modest changes in $E^{0'}$ were observed following substitution of surface nonpolar residues by polar residues[18]. As discussed in detail elsewhere[20,21], the reduction potential for the $[[3Fe–4S](Cys_3)]^{2-/3-}$ couple of native FdI is strongly pH dependent, with a limiting value E_{alk} (the reduction potential at pH > 9) = –444 mV and pK_{red} = 7.7, due to direct protonation of the reduced cluster. The oxidized cluster is too weak a base to protonate (pK_{ox} < 4). Mutations around the $[[3Fe–4S](Cys_3)]^{2-/3-}$ center have yielded only modest changes in $E^{0'}$ and pK[21].

We show that larger changes in $E^{0'}$ are induced by replacing Phe residues in FdI with His residues. Phe 2 is on the surface of the protein close to the $[[4Fe–4S](Cys_4)]^{2-}$ center, whereas Phe 25 is buried and located between the two clusters (Fig. 1). A previous F2Y mutation gave no change in $E^{0'}$, whereas a F25I mutation gave only a very small (–20 mV) change[12]. However, the possibility that His might produce much more pronounced effects is raised by a report[22] that substitution of Phe residues near the solvent-exposed $[[4Fe–4S](Cys_4)]^{2-/3-}$ center of the Fe protein of nitrogenase results in large changes in $E^{0'}$, with the 2(F135H) variant (the Fe protein is a dimer) giving the greatest change (~+120 mV). In that case, no structure was available for the Fe protein variant, making the data difficult to interpret. In principle, His *versus* Phe mutations could increase $E^{0'}$ by (i) attracting water to the vicinity of the cluster; (ii) introducing new NH–S bonds to the cluster; (iii) orienting an induced (positive) dipole toward the cluster; or (iv) introducing a positive charge near the cluster at pH values below the imidazole pK (ImH^+ / Im).

Here we report spectroscopic, voltammetric and high resolution structure determinations of the F2H and F25H variants of FdI. The His replacements introduce pH-dependent changes in $E^{0'}$ for $[[4Fe–4S](Cys_4)]^{2-/3-}$ that are far larger than those reported in any previous study. In addition, the F25H variant has a novel alteration in the proton-binding properties of the reduced $[[3Fe–4S](Cys_3)]^{3-}$ center.

Spectroscopy and electrochemistry

We compared the UV/Vis spectra of the F2H and F25H variants to those of native FdI, in their air-oxidized states ($[[3Fe–4S](Cys_3)]^{2-}$ and $[[4Fe–4S](Cys_4)]^{2-}$), and after anaerobic addition of dithionite (Fig. 2*a*,*b*). For the native protein, dithionite reduces the $[[3Fe–4S](Cys_3)]^{2-}$ center to the –3 oxidation state but does not result in reduction of $[[4Fe–4S](Cys_4)]^{2-}$, which has a very negative $E^{0'}$value[23]. By contrast, dithionite causes much more reversible bleaching of F2H and F25H, suggesting that the $E^{0'}$ values of the $[[4Fe–4S](Cys_4)]^{2-/3-}$ centers in these variants have increased. This was confirmed by electron paramagnetic resonance (EPR) spectroscopy, which shows that dithionite reduces the $[[4Fe–4S](Cys_4)]^{2-}$ centers of F2H and F25H by 33% and 90%, respectively.

The increases in $E^{0'}$ indicated by spectroscopy were quantified by solution cyclic voltammetry of F2H and F25H variants at pH 7.0 and 0 °C. For F2H, $E^{0'}$ for the $[[4Fe–4S](Cys_4)]^{2-/3-}$ center is –514 mV compared to –619 mV for native FdI — that is, a shift of +105 mV. As expected from the remote location of the mutation, there was no change for the $[[3Fe–4S](Cys_3)]^{2-/3-}$ center ($E^{0'}$ = –403 mV). In contrast, F25H lies between the two clusters, and both $E^{0'}$ values were dramatically altered. For $[[3Fe–4S](Cys_3)]^{2-/3-}$, $E^{0'}$ is –308 mV, an increase of ~100 mV, whereas for the $[[4Fe–4S](Cys_4)]^{2-/3-}$ center, which is closer to the mutated

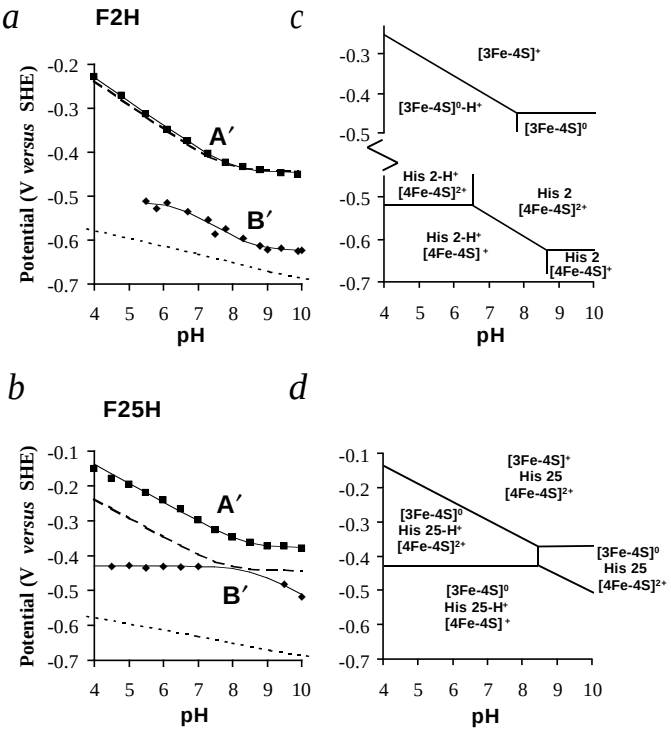

Fig. 3 The pH dependence of $E^{0'}$ values for $[[3Fe–4S](Cys_3)]^{2-/3-}$ and $[[4Fe–4S](Cys_4)]^{2-/3-}$ centers in F2H and F25H variants of FdI. ***a***, Data points and fits (solid lines) to Eq. 1 in F2H FdI. ***b***, Data points and fits (solid lines) to Eq. 1 in F25H FdI. Couple A′ is the $[[3Fe–4S](Cys_3)]^{2-/3-}$ center; couple B′, the $[[4Fe–4S](Cys_4)]^{2-/3-}$ center. The broken lines show best fits to the corresponding data obtained (pH 5.5–8.6) for native FdI from square-wave studies in solution, with the weak pH dependence for $[[4Fe–4S](Cys_4)]^{2/3-}$ being represented as a straight line[23]. The cell solution contained 60 mM mixed buffer, 0.1 M NaCl and 200 μg ml^{-1} polymyxin at 0 °C. The film potentials differ slightly from bulk solution but values can be determined very rapidly on the same sample over a wide range of electrode potential[29]. The errors in measuring potentials are ±5 mV, except for the region below pH 6 for the B' couple of F2H, where the error is ±10 mV. ***c***, Pourbaix diagrams showing the regions of existence of the various states of F2H under different conditions of electrode potential and pH[28]. For F2H, two separate diagrams are required to describe the states of the $[[3Fe–4S](Cys_3)]^{2-/3-}$ and the $[[4Fe–4S](Cys_4)]^{2-/3-}$ centers because His 2 interacts only with $[[4Fe–4S](Cys_4)]^{2-/3-}$. This diagram also describes the $[[3Fe–4S](Cys_3)]^{2-/3-}$ center of native FdI because that cluster was not affected by the F2H mutation. For the native protein, the cluster protonates directly, with a pK of 7.8 (ref. 21). ***d***, Pourbaix diagrams showing the regions of existence of the various states of F25H under different conditions of electrode potential and pH[28]. Unlike in F2H FdI, a single, more complex diagram is required to describe F25H because the ionization states of His 25 depend on the oxidation states of both clusters.

site, $E^{0'}$ is –408 mV, an increase of >200 mV and the largest change observed in any protein following site-directed mutagenesis of residues close to a $[[4Fe–4S](Cys_4)]^{2-/3}$ center.

The pH dependence of the potentials for native, F2H and F25H were recorded by protein film voltammetry (Fig. 3*a*,*b*). Couples A′ and B′ refer to the [[3Fe–4S](Cys3)]$^{2-/3-}$ and [[4Fe–4S](Cys4)]$^{2-/3-}$ transitions, respectively[24]. Normally, the [[4Fe–4S](Cys4)]$^{2-/3-}$ center in native FdI exhibits a weak pH dependence (~–15 mV per pH unit, measured over pH 5.5–8.6) that is probably due to ionizations at distant sites. However, both F2H and F25H exhibit strong pH dependencies attributable to coupling with a nearby protonatable group. The lines for F2H and F25H are fits to the general Eq. 1 for proton-coupled oxidation/reduction (Fig. 3 *a*,*b*)[25].

$$E^{0'}_{pH} = E^{0'}_{alk} + (RT / nF) \ln ((1 + (a_{H+})^{y} / K_{red}) / (1 + (a_{H+})^{y} / K_{ox}) \quad (1)$$

where $E^{0'}_{pH}$ is the value measured for a particular pH, $E^{0'}_{alk}$ is the reduction potential in the limit of high pH, a_{H+} is the H^+ activity, n is the number of electrons transferred (= 1), y is the number of protons transferred, K_{red} is the H^+ dissociation constant for the reduced species and K_{ox} is the H^+ dissociation constant for the oxidized species. The terms R, T and Faraday constant (F) have their usual meanings.

For the $[[4Fe–4S](Cys_4)]^{2-/3-}$ center of F2H, a good fit to the data (Fig. 3) was obtained with pK_{red} = 8.5 and $E^{0'}_{alk}$ = –625 mV. Overlap from the oxidation peak of the $[3Fe–4S]^{0/2-}$ couple restricted the reliability of data points at values below pH 6. However, an ionization associated with the oxidized $[[4Fe–4S](Cys_4)]^{2-}$ center is apparent, and we obtained a best fit with pK_{ox} = 6.5 and $E^{0'}_{acid}$ (the limiting potential at pH values below pK_{ox}) = –514 mV. How a [4Fe–4S] cluster can protonate directly is not obvious, and there are no examples of natural clusters of this type showing such a strong pH dependency of $E^{0'}$. Therefore, the pH dependence of the $[[4Fe–4S](Cys_4)]^{2-/3-}$ potential is due to protonation/deprotonation of the introduced His 2. The pK of His 2 is sensitive to the cluster oxidation level, where, as expected, adding an electron to the cluster makes adding a proton to the neighboring His easier. For F25H, the reduction potential for the $[[4Fe–4S](Cys_4)]^{2-/3-}$ center is increased further, and a fit to the data yields $E^{0'}_{acid}$ = –432 mV and pK_{ox} = 8.5, with $E^{0'}_{alk} < –550$ mV and $pK_{red} > 10$. If the pH dependence in this case is also caused by protonation/deprotonation of the introduced His 25, the simplest explanation is that His 25 is protonated below pH 8.5. The large positive shift in reduction potential in the low pH region is unprecedented and has not been observed for any other mutations made in this region.

The pH dependence for the $[[3Fe–4S](Cys_3)]^{2-/3-}$ center in F25H resembles that normally observed for the native protein and all other mutants studied, except that the data points and the fit line lie ~100 mV more positive in potential. Also, pK_{red} is quite high (8.4) and corresponds closely with pK_{ox} = 8.5 for the $[[4Fe–4S](Cys_4)]^{2-/3-}$ center, suggesting a common origin — that is, protonation of His 25. Unlike native FdI, the circular dichroism (CD) spectrum of F25H does not change to that of the protonated cluster when the pH is decreased from 8.0 to 6.0 (Fig. 4*a*). Therefore, the $[[3Fe–4S](Cys_3)]^{3-}$ center of F25H is not directly protonated[26].

To investigate this further, the temperature dependence of $E^{0'}$ for the $[[3Fe–4S](Cys_3)]^{2-/3-}$center in F25H and native FdI was measured at pH values above and below pK_{red} (Fig. 4*b*). Under alkaline conditions, the higher reduction potential for F25H, relative to native FdI, is due to a more favorable ΔS^0 and a slightly more favorable ΔH^0. A striking difference is observed at pH 5.0, where a proton is taken up from bulk water. For native FdI, there is little difference in ΔH^0 compared to that observed at high pH and protonation is associated with a favorable (positive) ΔS^0. The opposite is true for F25H, where reduction at low pH has a more unfavorable ΔS^0 and a favorable (negative) ΔH^0 compared to values at high pH. The difference between native FdI and F25H, $\Delta(\Delta H^0)$ = –33 kJ mol^{-1} and $\Delta(T\Delta S^0)$ = –26 kJ mol^{-1}, reflects the thermodynamics of internal proton transfer from the $[[3Fe–4S](Cys_3)]^{3-}$ to the new site of protonation. The $\Delta(\Delta H^0)$ value is consistent with transfer from a μ_2 S (low proton affinity) to an imidazole N (high proton affinity)[27], whereas the unfavorable $\Delta(T\Delta S^0)$ reflects the structural ordering (analogous to Born ion solvation entropy), with charge separation as the proton is moved away from the reduced cluster.

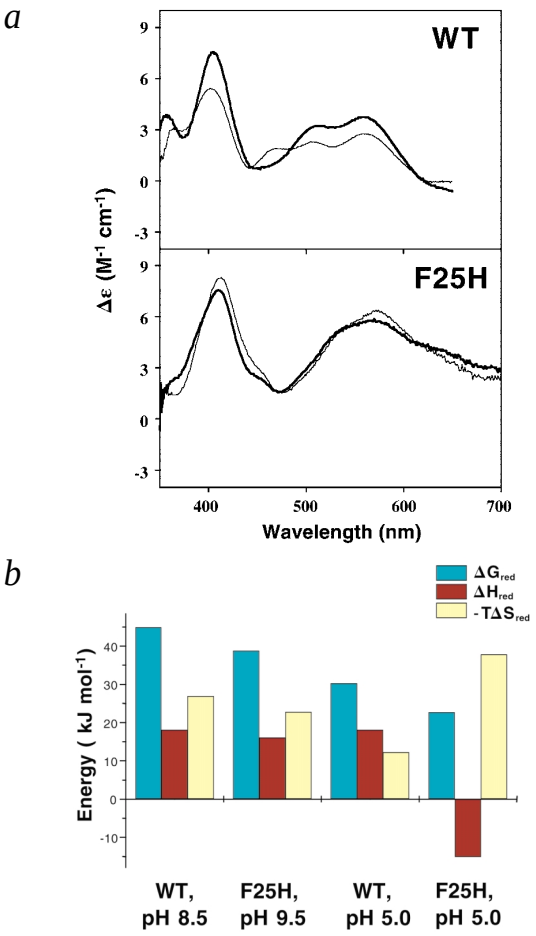

Fig. 4 Protonation of His 25, not of the cluster, causes the pH dependence of reduction potential of the $[[3Fe–4S](Cys_3)]^{2-/3-}$ center in F25H. ***a***, CD spectra of native FdI and F25H FdI reduced by sodium dithionite at different pH values: pH 6.0 (thin line) and pH 8.0 (thick line). All samples were in 50 mM TAPS, 50 mM PIPES and 2 mM sodium dithionite. The observed spectral change for native FdI is due to protonation of a μ_2-S for the $[[3Fe–4S](Cys_3)]^{3-}$ center[26]. ***b***, The thermodynamics of the one-electron reduction of the $[[3Fe–4S](Cys_3)]^{2-}$ cluster as measured from the temperature dependence of $E^{0'}$. The total free energy change (ΔG) is shown along with its enthalpic (ΔH) and entropic ($-T\Delta S_{red}$) components. Data are for native FdI at pH 8.5 (no associated proton transfer), F25H FdI at pH 9.5 (no associated proton transfer), wild type FdI at pH 5.0 (associated protonation of the cluster) and F25H FdI at pH 5.0 (associated protonation of H25). Errors are ±0.5 kJmol^{-1} for ΔG_{red} and ±2 kJ mol for ΔS_{red} and ΔH_{red}.

The results for F2H and F25H are shown as Pourbaix diagrams[28], which depict (in 'potential/pH space') the conditions for existence of the different redox and protonation states of the clusters and the introduced His residues (Fig. 3*c*,*d*). For the F25H variant, the pK of His 25 spans a pH range >6 units depending on the oxidation states of the two clusters even though it is not a ligand. Thus, when both clusters are oxidized, pK < 4, whereas with both clusters reduced, pK > 10; the protonated state is stabilized by the increasing negative charge on the centers when they are reduced. Under conditions that the protein contains $[[3Fe–4S](Cys_3)]^{3-}$ (reduced) and $[[4Fe–4S](Cys_4)]^{2-}$ (oxidized), the pK is 8.5.

F2H crystal structure

The crystal structure of F2H FdI (Fig. 1*a*) is similar to that of the native protein — that is, main chain atoms superimpose with a root mean square (r.m.s.) deviation of 0.27 Å. The His 2 side chain adopts the same conformation as Phe 2 and acquires two hydrogen bonds, one from Asp 41 and one from Glu 46, exhibiting two new conformations of equal occupancy compared to native FdI. Because a previous E46A mutation did not change the reduction potential[12], the movement of that side chain is not responsible for the changes observed here. The position of His 2 places it directly adjacent to the $[4Fe–4S]^{2+/+}$ cluster, with the shortest contacts being 3.6 Å between both Nδ1 and Cγ and inorganic sulfur. In the F2H mutant, $E^{0'}$ for the $[[4Fe–4S](Cys_4)]^{2-/3-}$ center shows a sigmoidal variation with pH and is significantly increased at all pH values compared to native FdI. No effect is seen at the $[[3Fe–4S](Cys_3)]^{2-/3-}$ center, consistent with its distal location relative to His 2. In the vicinity of the $[[4Fe–4S](Cys_4)]^{2-}$ center, the NH–S hydrogen bonding does not change, and the solvent accessibility of the cluster is not altered. Hence, the increase in potential cannot be due to a change in amide or solvent dipoles in the oxidized form. Rather, the major effect results from the introduction of positive charge adjacent to the cluster due to protonation of the His. The smaller increase in $E^{0'}$ when His is neutral may occur by directing the $H^{\delta+}–N^{\delta-}$ dipole toward the reduced form of the cluster.

F25H crystal structure

In native FdI, Phe 25 is a buried hydrophobic residue sandwiched between the $[[4Fe\ 4S](Cys_4)]^{2-}$ and $[[3Fe–4S](Cys_3)]^{2-}$ centers. Consequently, in the structure of F25H FdI (Fig. 1*b*), the introduced His 25 side chain makes six contacts <4 Å to the clusters: two to inorganic sulfur atoms of the $[[4Fe–4S](Cys_4)]^{2-}$ center, two to Sγ of Cys 20 (a 4Fe cluster ligand) and two to Sγ of Cys 16, which is a 3Fe cluster ligand (Fig. 1*b*). Because the structures are otherwise very similar (the r.m.s. deviation of main chain atoms is 0.23 Å), there is no change in NH–S hydrogen bonding or solvent accessibility of the clusters in this mutant. Two tightly bound H_2O molecules shift slightly so that one of them forms a hydrogen bond with Nδ1 of His 25 (Fig. 1*b*).

In F25H FdI, the reduction potentials of both clusters are raised (Fig. 3). The major factor altering $E^{0'}$ is protonation of His 25, which occurs for the reduced $[[3Fe–4S](Cys_3)]^{3-}$ center at pH values below the pK of 8.4 and for the reduced $[[4Fe–4S](Cys_4)]^{3-}$ center throughout the entire pH range. By contrast, for the fully oxidized protein, His 25 is unprotonated for all pH values >4 (the region in which the structure was determined). From this structure, the much greater effect of His 25 protonation on $E^{0'}$ for the $[[4Fe–4S](Cys_4)]^{2-/3-}$ center can be anticipated because there are twice as many short-range contacts (four at distances <4 Å) to $[[4Fe–4S](Cys_4)]^{2-}$ *versus* two to the $[[3Fe–4S](Cys_3)]^{2-}$ center (there are only two such contacts in F2H). At high pH, where His 25 is neutral when the $[[4Fe–4S](Cys_4)]^{2-/3-}$ center is oxidized, the positive shift in $E^{0'}$ for the $[[3Fe–4S](Cys_4)]^{2-/3-}$ center must have a more subtle origin. The imidazole ring of His 25 is stacked directly over Sγ of the $[[3Fe–4S](Cys_3)]^{2-}$ center (Fig. 1*b*). Except for one hydrogen bond to water, His 25 resides in a hydrophobic cavity with contacts to Val 17, Ile 34 and Ile 81, and neither the Nδ1 nor the Nε2 atom is oriented such that new NH–S interactions occur. However, this provides an important way to raise $E^{0'}$, because a small realignment of the neutral imidazole ring to produce a compensatory $H^{\delta+}–N^{\delta-}$ dipole is all that is required to stabilize the $[[3Fe–4S](Cys_3)]^{3-}$ form.

Conclusions

Large increases in [Fe–S] reduction potential (100 to 200 mV *versus* SHE) have been observed following the introduction of single His residues close to the Fe–S clusters of *A. vinelandii* FdI. High-

Table 1 Data collection and refinement statistics

Structure	F2H FdI	F25H FdI
Unit cell		
Space group	$P4_12_12$	$P4_12_12$
Unit cell parameters		
$\alpha = \beta = \gamma$ (°)	90	90
a = b (Å)	55.38	55.22
c (Å)	92.78	92.72
Data collection		
Resolution range (Å)	50.0–1.62	50.0–1.75
Total observations	225,694	202,912
Independent reflections	19,082	15,118
Completeness (%)[1]	99.9 (100)	99.7 (100)
R_{sym} (I)[1]	0.072 (0.642)	0.072 (0.606)
I / σ (I)[1]	9.6 (2.04)	8.8 (2.17)
Last shell resolution (Å)	1.65–1.62	1.78–1.75
Refinement		
Resolution range (Å)	39.2–1.62	39.1–1.75
Reflections > 0.0 σ_F	18,542	14,617
R_{free} (5% of data)	0.244	0.232
R-factor	0.207	0.203
R.m.s. deviations		
Bond lengths (Å)	0.005	0.006
Bond angles (°)	1.79	1.76
Number of atoms		
Protein	840	840
[4Fe–4S]	8	8
[3Fe–4S]	7	7
Water	176	165
Average B-factor (Å^2)		
Protein	22.0	23.0
[4Fe–4S]	19.0	21.5
[3Fe–4S]	18.0	20.1
Water	36.6	38.9

[1]Number in parentheses is for the last resolution shell.

resolution X-ray structures of F2H and F25H variants in their oxidized forms and CD in the reduced forms reveal that these changes cannot be attributed to increased solvent accessibility of the clusters, reorientation of backbone amide dipoles, or reorientation of existing (or introduction of new) NH–S bonds. The variation of reduction potential with pH and temperature and the crystal structures lead to the conclusion that the largest increases in $E^{0'}$ result from the introduction of positive charge due to protonation of the His. The data also reveal that the pK of the introduced His is greatly influenced by the oxidation state of the clusters (>6 pH units). The smaller increases observed when the His is neutral are proposed to arise by the ability of the imidazole ring to tilt and direct a $H^{\delta+}$–$N^{\delta-}$ dipole toward the reduced form of the cluster. For F25H, both the $[[3Fe–4S](Cys_3)]^{2-/3-}$ and the $[[4Fe–4S](Cys_4)]^{2-/3-}$ centers are strongly coupled to protonation of the imidazole, and the $[[3Fe–4S](Cys_3)]^{3-}$ center is no longer protonated.

Methods

Construction and characterization of F2H and F25H variants. The F2H and F25H variants of *A. vinelandii* FdI were constructed, expressed in their native background and purified as described[18]. UV-visible absorption spectra were recorded on a Hewlett Packard 8452A diode array spectrophotometer. CD spectra were obtained using a Jasco J-500C spectropolarimeter. EPR spectra were obtained using a Bruker ESP300E spectrometer, interfaced with an Oxford liquid helium cryostat. Experimental conditions are as follows: microwave power was 10 mW (native FdI) and 0.4 mW (for F2H and F25H); microwave frequency, 9.59 GHz; temperature, 10 K; amplitude, 5 G; and protein concentration, 108 μM (native FdI) and 84 μM (F2H and F25H). These conditions were chosen for spin quantitation because the EPR signal is linearly proportional to [power]$^{1/2}$. Cu^{2+}-EDTA (85 μM) was used as a standard and recorded at the same EPR settings and temperature, where the signal also increases as a linear function of [power]$^{1/2}$. The concentration of spin was calculated by double integration of the signal over the entire field sweeps. Cyclic voltammetry (both solutions and film) was carried out as described, using a pyrolytic graphite 'edge' electrode[18,24]. A nonisothermal cell was used, in which the standard calomel reference electrode was maintained at 25 °C while the cell solution was varied between 0 °C and 30 °C.

Tetragonal FdI crystals were grown as described[18]. The protein concentration for both F2H and F25H was 11 mg ml^{-1} in 4 μl of 1.2 M ammonium sulfate and 0.4 M Tris-HCl, pH 7.4. The entire data collection was done at 100 K. The structures of F2H and F25H were determined as described[18]. Unbiased $2|F_o| - |F_c|$ and $|F_o| - |F_c|$ electron density maps clearly revealed the positions of the His side chains for the F2H and F25H replacements. The structures were refined to 1.62 Å resolution with R-factor = 0.207 and R_{free} = 0.244 for F2H, and to 1.75 Å resolution with R-factor = 0.203 and R_{free} = 0.232 for F25H (Table 1). The isotropic B-factors were refined at the same time and are included in the PDB diposition. The B-factors of His 2 and His 25 are comparable to Phe 2 and Phe 25.

Coordinates. Coordinates for the F2H and F25H FdI structures have been deposited with Protein Data Bank (accession codes 1F5B and 1F5C, respectively).

Acknowledgments

The authors wish to acknowledge V. Roberts and L. Noodleman at The Scripps Research Institute, and M. Gunner, City College, New York, and J. Hirst, MRC, Cambridge for helpful discussions. G. Murcott (Oxford) assisted in some of the experiments. We also thank T.L. Poulos and H. Li at University of California-Irvine for use of laboratory facilities for X-ray crystallography. This work was funded by grants from UK EPSRC and BBSRC to F.A.A. and NIH grants to C.D.S. and B.K.B.

Barbara K. Burgess died unexpectedly on December 30, 2001. We would like to pay tribute to her many contributions to science; in particular her studies of the proteins and cofactors involved in biological nitrogen fixation, and her elucidation of many important properties of iron-sulfur clusters.

Correspondence should be addressed to Susan Bryant. *email: svbryant@uci.edu*

Received 29 May, 2001; accepted 28 November, 2001.

1. Beinert, H. *J. Biol. Inorg. Chem.* 5, 2–15 (2000).
2. Bertini, I., Gori-Savellini, G. & Luchinat, C. *J. Bio. Inorg. Chem.* 2, 114–118 (1997).
3. Przysiecki, C.T., Meyer, T.E. & Cusanovich, M.A. *Biochemistry* 24, 2542–2549 (1985).
4. Stephens, P.J., Jollie, D.R. & Warshel, A. *Chem. Rev.* 96, 2491–2513 (1996).
5. Heering, H.A., Bulsink, Y.B.M., Hagen, W.R. & Meyer, T.E. *Eur. J. Biochem.* 232, 811–817 (1995).
6. Iwagami, S.G. *et al. Protein Sci.* 4, 2562–2572 (1995).
7. Soriano, A., Li, D., Bian, S., Agarwal, A. & Cowan, J.A. *Biochemistry* 35, 12479–12486 (1996).
8. Denke, E. *et al. J. Biol. Chem.* 271, 9085–9093 (1998).
9. Schroter, T. *et al. Eur. J. Biochem.* 255, 100–106 (1998).
10. Eidsness, M.K. *et al. Biochemistry* 38, 14803–14809 (1999).
11. Backes, G. *et al. J. Am. Chem. Soc.* 113, 2055–2064 (1991).
12. Shen, B. *et al. J. Biol. Chem.* 269, 8564–8575 (1994).
13. Mauk, A.G. & Moore, G.R. *J. Biol. Inorg. Chem.* 2, 119–125 (1997).
14. Náray-Szabó, G. *J. Biol. Inorg. Chem.* 2, 135–138 (1997).
15. Warshel, A., Papazyan, A. & Muegge, I. *J. Biol. Inorg. Chem.* 2, 143–152 (1997).
16. Moore, G.R. *FEBS Lett.* 161, 171–175 (1983).
17. Schejter, A. & Eaton, W.A. *Biochemistry* 23, 1081–1084 (1984).
18. Chen, K. *et al. J. Biol. Chem.* 274, 36479–36487 (1999).
19. Li, J., Nelson, M.R., Peng, C.Y., Bashford, D. & Noodleman, L. *J. Phys. Chem.* 102, 6311–6324 (1998).
20. Shen, B. *et al. J. Biol. Chem.* 268, 25928–25939 (1993).
21. Chen, K. *et al. Nature* 405, 814–817 (2000).
22. Ryle, M.J., Lanzilotta, W.N. & Seefeldt, L.C. *Biochemistry* 35, 9424–9434 (1996).
23. Iismaa, S.E. *et al. J. Biol. Chem.* 266, 21563–21571 (1991).
24. Armstrong, F.A., Butt, J.N. & Sucheta, A. *Methods Enzymol.* 227, 479–500 (1993).
25. Dutton, P.L. & Wilson, D.F. *Biochim. Biophys. Acta* 346, 165–212 (1974).
26. Stephens, P.J. *et al. Biochemistry* 30, 3200–3209 (1991).
27. Hunter, E.P. & Lias, S.G. *J. Phys. Chem. Ref. Data* 27, 413 (1998).
28. Delahay, P., Pourbaix, M. & Van Rysselberghe, P. *J. Chem. Educ.* 27, 683 – 688 (1950).
29. Armstrong, F.A., Heering, H.A. & Hirst, J. *Chem. Soc. Rev.* 26, 169–179 (1997).